is the case in all complexes and molecules where X is a more electronegative ligand (substituent) than the central atom of fragment A to which the ligands are bound. These are usually also the chemically relevant orbitals, and it is often sufficient to compare the structures by starting with an electron count where all A-X bonding levels are already filled to avoid this problem. Even so, with more than two sets of energy levels the question does arise as to whether the enerties of the relevant structures should be compared at constant Fermi level or by ensuring that there are the same number of electrons in each structure to be compared. For the case of the two cis ligands of the octahedron, should then the properties of the merged density of states $[(O_h\text{-}ML_6) + (C_{2v}\text{-}ML_4)]$ be compared with the merged density of states $[2E(C_{4v}\text{-}ML_5)]$, or should the energies $E(O_h\text{-}ML_6)$, $E(C_{2v}\text{-}ML_4)$, and $2E(C_{4v}\text{-}ML_5)$ be separately evaluated at each electron count and then compared?

If the orbitals of the isolated ligand X lie energetically between the chemically important orbitals of the unit A or AX, the energy as a function of orbital filling has to be calculated for the case where the orbitals of the fragment A or AX are merged with the orbitals of the isolated ligand; otherwise, the pair potential exhibits wildly oscillating (and chemically meaningless) behavior in this region. This implies that $[E(AX + X)](x)$ or $[E(A + 2X)](x)$ has to be calculated instead of $[E(AX)](x)$ or $[E(A)](x)$. This is the case too for the pair potential between two vertices in the octahedral cluster B_6H_6 (here, A = C_{2v}-B_4H_4, X = BH). Here we need to calculate the pair potential as

$$\phi(x) = [E(B_6H_6)](x) + [E(B_4H_4 + 2BH)](x) - 2[E(B_5H_5 + BH)](x)$$

As discussed in the text, this is a case where the total number of close contacts is only maintained if two separated BH units are used in the second term.

Predictions from the method of moments as to the shapes expected for the $\phi(x)$ curves may sometimes be made. If two atoms first see each other via a self-returning walk of length 4, then the pair potential should exhibit four nodes, on the basis of the same type of argument employed for the energy difference plots themselves. Indeed, this expected correlation between $\Delta E(x)$ and $\phi(x)$ is found in Figure 1. However the sign of $\phi(x)$ may often not be as easily predicted. For the comparison of two densities of states, then the existing arguments show that the system with the larger fourth moment will be the more stable one for early and late orbital occupancies. But determination of $\phi(x)$ involves more than two sets of energy levels. If two merged sets of energy levels are used, then no ambiguity arises, but if three unmerged sets are used in the comparison, as we describe above, then the ideas associated with the moments method make no predictions as to the resultant sign of $\phi(x)$.

Appendix II

All calculations were performed by using the extended Hückel method. The parameters used are given in Table II. For the calculations of AX_n systems (Figures 4 and 6-10) Cr parameters for s/p, d, and s/p/d orbitals were used. To reduce the ligand-ligand interaction in these systems, the hydrogen Slater type orbital exponent was varied from 1.3 to 2.425 (the value used for fluorine 2s). Qualitatively similar results were obtained by using the standard parameters for H 1s and setting the ligand-ligand overlap integrals equal to zero. For the calculation shown in Figures 11-13 the usual Cr, H, and B parameters were used (Table II).

All central atom (A or M)-hydrogen distances were kept to 1.8 Å; for calculations involving M-M bonds a M-M distance of 2.49 Å was used. The B-B and B-H distances were 1.75 and 1.2 Å, respectively.

Contribution from the Department of Chemistry, University of Maine, Orono, Maine 04469, and Departments of Physics and Chemistry, Bowdoin College, Brunswick, Maine 04011

Photoluminescence and Electronic Structure of $Tl[Au(CN)_2]$: Evidence for Relativistic Effects in Thallium-Gold and Gold-Gold Interactions

Zerihun Assefa,[†] Frank DeStefano,[†] Mohammad A. Garepapaghi,[‡] Joseph H. LaCasce, Jr.,[‡] Steve Ouellette,[†] Michael R. Corson,[‡,§] Jeffrey K. Nagle,*[,∥] and Howard H. Patterson*[,†]

Received April 10, 1990

Experimental results of a study of the photoluminescence of microcrystalline $Tl[Au(CN)_2]$ as a function of temperature (1.7-400 K) and magnetic field (0-6 T) are described. These results, along with relativistically modified extended Hückel calculations, provide evidence that covalent Tl-Au interactions alter its spectroscopic properties in comparison with isostructural $Cs[Au(CN)_2]$. Specifically, the absorption and luminescence of $Tl[Au(CN)_2]$ appear at lower energies than for $Cs[Au(CN)_2]$, and a comparison of the luminescence spectra and lifetimes for the two compounds reveals evidence for an increased rate of intersystem crossing in $Tl[Au(CN)_2]$ relative to $Cs[Au(CN)_2]$. Both effects are reflective of covalent Tl-Au interactions in $Tl[Au(CN)_2]$. The electronic structure calculations clearly demonstrate the covalency of both the Tl-Au and Au-Au interactions in $Tl[Au(CN)_2]$ and reveal specific orbital contributions responsible for these interactions. Relativistic effects are shown to play an important role in the Tl-Au and Au-Au bonding.

Introduction

The tendency of certain 5d elements such as Ir, Pt, and Au to bond to 6p elements such as Tl and Pb in some compounds has recently been demonstrated.[1] It is likely that relativistic effects play an important role in this phenomenon by altering the energies and sizes of the valence orbitals involved as compared to the nonrelativistic situation.[1,2] X-ray structural analysis of single crystals has been invaluable in establishing the presence of such bonding,[3] but little is known about the detailed electronic structures of these compounds. Spectroscopic investigations, including both electronic absorption and luminescence, and electronic structure

[†] University of Maine.
[‡] Department of Physics, Bowdoin College.
[§] Present address: Physical Sciences, Inc., 603 King St., Alexandria, VA 22314.
[∥] Department of Chemistry, Bowdoin College.

(1) See for example Ziegler, T.; Nagle, J. K.; Snijders, J. G.; Baerends, E. J. *J. Am. Chem. Soc.* **1989**, *111*, 5631-5635 and references therein.
(2) (a) Pyykkö, P. *Chem. Rev.* **1988**, *88*, 563-594. (b) Pyykkö, P. In *Methods in Computational Chemistry*; Wilson, S., Ed.; Plenum Press: New York, 1988; Vol. 2, pp 137-221. (c) Schwerdtfeger, P.; Dolg, M.; Schwarz, G. A.; Bowmaker, W. H. E.; Boyd, P. D. W. *J. Chem. Phys.* **1989**, *91*, 1762-1774. (d) Ziegler, T.; Snijders, J. G.; Baerends, E. J. *J. Chem. Phys.* **1981**, *74*, 1271-1284. (e) Balasubramanian, K. *J. Phys. Chem.* **1989**, *93*, 6585-6596. (f) Pyykkö, P.; Desclaux, J.-P. *Acc. Chem. Res.* **1979**, *12*, 276-281. (g) Schwerdtfeger, P.; Boyd, P. D. W.; Bowmaker, G. A.; Mack, H. G.; Oberhammer, H. *J. Am. Chem. Soc.* **1989**, *111*, 15-23. (h) Schwerdtfeger, P.; Boyd, P. D. W.; Burrell, A. K.; Robinson, W. T.; Taylor, M. J. *Inorg. Chem.* **1990**, *29*, 3593-3597.
(3) Nagle, J. K.; Balch, A. L.; Olmstead, M. M. *J. Am. Chem. Soc.* **1988**, *110*, 319-321.

0020-1669/91/1330-2868$02.50/0

calculations[1] promise to help alter this situation. Here we report a detailed spectroscopic and molecular orbital study of solid Tl[Au(CN)$_2$]. This substance is of specific interest because Au is predicted to have optimum relativistic bonding effects,[2f] and both Tl–Au and Au–Au interactions are present in this compound.

It is known that for compounds of the d^{10} ions Cu(I), Ag(I), and Au(I) substantial $(n + 1)$s and $(n + 1)$p mixing with the nd orbitals facilitates metal–metal bond formation.[4-6] Previous theoretical studies of molecules containing two d^{10} centers such as Cu(I)–Cu(I),[5a,7] Ag(I)–Ag(I),[7] and Pt(0)–Pt(0)[6] have helped to determine whether metal–metal interactions are present. Au(I) compounds in particular are known to form dimers and higher nuclearity clusters—including polymeric chains—in which the repeat unit is a linear AuL_2 group with direct Au–Au interactions.[5b,8-10]

The existence of Au–Au interactions in K[Au(CN)$_2$][11] and Cs[Au(CN)$_2$][12]—both of which contain two-dimensional arrays of Au atoms—has led to photoluminescence studies[13-16] designed to probe the nature of these interactions. Since neither the relatively low-energy absorption bands nor the luminescence associated with these bands is observed in the absence of such close Au–Au contacts, a model involving Au 5d, 6s, and 6p orbital overlaps has been proposed to account for these optical properties.[15] This model has been extended to explain the effects of a magnetic field on the low-temperature photoluminescence lifetimes and spectra of Cs[Au(CN)$_2$].[16] Recent studies have found that some Au(I) dimers[10g,h] and a tetramer[10i] luminescence in fluid solution at room temperature.

Tl[Au(CN)$_2$] is isostructural with Cs[Au(CN)$_2$].[12] However, in addition to being within 3.10 Å of two adjacent Au atoms, one of the three crystallographically distinct Au sites is within 3.50 Å of two adjacent Tl atoms. Vibrational spectroscopic studies of this compound[17] point to the presence of significant Au–Tl interactions. A detailed analysis of the photoluminescence lifetimes and spectra of this compound as a function of temperature and magnetic field strength is here reported for the first time and compared to that developed previously for Cs[Au(CN)$_2$].[13-16,18]

Table I. Extended Hückel Relativistic Parameters[a]

orbital	$-H_{ij}$, eV	slater exponent
Au 6s	7.94 (6.01)	2.12 (1.76)
Au 6p	3.47 (3.21)	1.50 (1.36)
Au 5d	12.37 (14.18)	3.47 (3.56)
C 2s	19.39 (19.38)	1.58 (1.58)
C 2p	11.03 (11.07)	1.43 (1.44)
N 2s	26.25 (26.22)	1.84 (1.89)
N 2p	13.84 (13.84)	1.73 (1.73)
Tl 6s	12.22 (9.83)	2.53 (2.19)
Tl 6p	5.12 (5.23)	1.70 (1.66)
Tl 5d	22.90 (26.35)	4.01 (4.10)
Pt 6s	7.73 (5.93)	2.07 (1.73)
Pt 6p	4.13 (4.05)	1.69 (1.60)
Pt 5d	11.20 (12.97)	3.30 (3.41)

[a] Data in parentheses are nonrelativistic values.

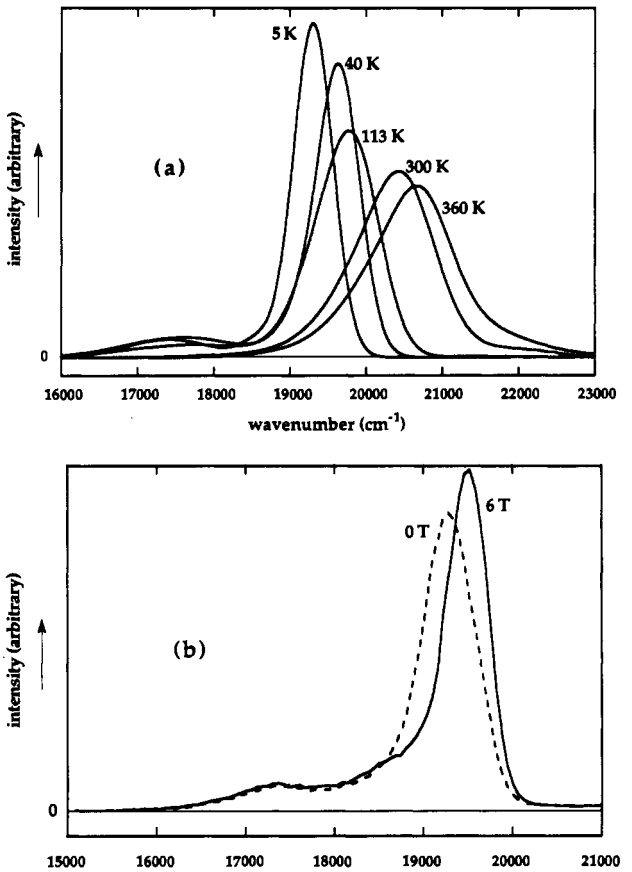

Figure 1. (a) Luminescence spectra of microcrystalline Tl[Au(CN)$_2$] from 5 to 360 K. The area of each spectrum was arbitrarily held constant to facilitate viewing. (b) Luminescence spectra of microcrystalline Tl[Au(CN)$_2$] at 4.2 K at 0 T (solid line) and at a magnetic flux density of 6 T (dashed line).

In addition a relativistic, extended Hückel calculation (using Slater exponents and valence-state ionization potentials given elsewhere[19]) on the electronic structure of Tl[Au(CN)$_2$] is reported. Results are reported also for $Tl_2Pt(CN)_4$ because it has been found to possess direct Pt–Tl bonds,[3] and a recently reported relativistic density-functional calculation of its electronic structure[1] provides an important calibration point for the simpler extended Hückel calculations. A preliminary account of this work has appeared,[20] including a comparison with $Tl_2Pt(CN)_4$, which shows low-temperature luminescence behavior similar to that observed for Tl[Au(CN)$_2$].

(4) Jansen, M. *Angew. Chem., Int. Ed. Engl.* **1987**, *26*, 1098–1110.
(5) (a) Mehrotra, P.; Hoffmann, R. *Inorg. Chem.* **1978**, *17*, 2187–2189. (b) Jiang, Y.; Alvarez, S.; Hoffmann, R. *Inorg. Chem.* **1985**, *24*, 749–757.
(6) Dedieu, A.; Hoffmann, R. *J. Am. Chem. Soc.* **1978**, *100*, 2074–2079.
(7) Cotton, F. A.; Feng, X.; Matuz, M.; Poli, R. *J. Am. Chem. Soc.* **1988**, *110*, 7077–7083.
(8) (a) Jones, P. G. *Gold Bull.* **1981**, *14*, 102–118, 159–166; **1983**, *16*, 114–124; **1986**, *19*, 46–57. (b) Uson, R.; Laguna, A. *Coord. Chem. Rev.* **1986**, *70*, 1–50. (c) Melnik, M.; Parish, R. V. *Coord. Chem. Rev.* **1986**, *70*, 157–257.
(9) Hall, K. P.; Mingos, D. M. P. *Prog. Inorg. Chem.* **1984**, *32*, 237–325.
(10) Recent studies: (a) Khan, M. N. I.; King, C.; Heinrich, D. D.; Fackler, J. P., Jr.; Porter, L. C. *Inorg. Chem.* **1989**, *28*, 2150–2154. (b) Khan, M. N. I.; Fackler, J. P., Jr.; King, C.; Wang, J. C.; Wang, S. *Inorg. Chem.* **1988**, *27*, 1672–1673. (c) Schmidbaur, H.; Graf, W.; Müller, G. *Angew. Chem., Int. Ed. Engl.* **1988**, *27*, 417–419. (d) Moore, L. S.; Parish, R. V.; Uson, R.; Laguna, A.; Laguna, M.; Fraaile, M.; Nieves-Fraile, J. *J. Chem. Soc., Dalton Trans.* **1988**, 23–26. (e) Vogler, A.; Kunkley, H. *Chem. Phys. Lett.* **1988**, *150*, 135–137. (f) Jaw, H.-R.; Savas, M. M.; Rogers, R. D.; Mason, W. R. *Inorg. Chem.* **1989**, *28*, 1028–1037. (g) King, C.; Wang, J. C.; Khan, M. N. I.; Fackler, J. P., Jr. *Inorg. Chem.* **1989**, *28*, 2145–2149. (h) Che, C. M.; Kwong, H. L.; Yam, V. W. W.; Cho, K. C. *J. Chem. Soc., Chem. Commun.* **1989**, 885–886. (i) Vogler, A.; Kunkley, H. *Chem. Phys. Lett.* **1988**, *150*, 135–137. (j) Khan, M. N. I.; Wang, S.; Fackler, J. P., Jr. *Inorg. Chem.* **1989**, *28*, 3579–3588.
(11) Rosenzweig, A.; Cromer, D. T. *Acta Crystallogr.* **1959**, *12*, 709–712.
(12) Blom, N.; Ludi, A.; Bürgi, H.-B.; Tichy, K. *Acta Crystallogr., Sect. C: Cryst. Struct. Commun.* **1984**, *40*, 1767–1769.
(13) Patterson, H. H.; Roper, G.; Biscoe, J.; Ludi, A.; Blom, N. *J. Lumin.* **1984**, *31–32*, 555–557.
(14) Nagasundaram, N.; Roper, G.; Biscoe, J.; Chai, J. W.; Patterson, H. H.; Blom, N.; Ludi, A. *Inorg. Chem.* **1986**, *25*, 2947–2951.
(15) Markert, J. T.; Blom, N.; Roper, G.; Perregaux, A. D.; Nagasundaram, N.; Corson, M. R.; Ludi, A.; Nagle, J. K.; Patterson, H. H. *Chem. Phys. Lett.* **1985**, *118*, 258–262.
(16) LaCasce, J. H., Jr.; Turner, W. A.; Corson, M. R.; Dolan, P. J., Jr.; Nagle, J. K. *Chem. Phys.* **1987**, *118*, 289–294.
(17) Stammreich, H.; Chadwick, B. M.; Frankiss, S. G. *J. Mol. Struct.* **1967–1968**, *1*, 191–196. Chadwick, B. M.; Frankiss, S. G. *J. Mol. Struct.* **1976**, *31*, 1–9.
(18) Blom, N. Thesis, University of Bern, 1983.
(19) Pyykkö, P.; Lohr, L. L. *Inorg. Chem.* **1981**, *20*, 1950–1959.
(20) Nagle, J. K.; LaCasce, J.; Corson, M. R.; Dolan, P. J., Jr.; Assefa, Z.; Patterson, H. H. *Mol. Cryst. Liq. Cryst.* **1990**, *181*, 359–366.

Experimental Section

$Tl[Au(CN)_2]$ was prepared by slow addition of $TlNO_3$ to aqueous solutions of $K[Au(CN)_2]\cdot 2H_2O$ (Spex). The bright canary yellow precipitate was filtered and washed with several portions of cold water and dried and stored in a vacuum desiccator.

Photoluminescence spectra and lifetime data were obtained with equipment and procedures described previously.[16] A Laser Science Inc. nitrogen-pumped BBQ dye with a maximum output at 25 100 cm^{-1} was used for the lifetime measurements. An Oriel 5755 band-pass filter was used to select the luminescence in the 19 000–21 000-cm^{-1} region. Measurements of luminescence spectra were obtained by filtering the output from a mercury lamp through an Oriel 5181 band-pass filter (27 400-cm^{-1} maximum throughput). A Cryomagnetics magnet was used to produce magnetic fields up to 6 T. Three lifetime measurements were made at the University of Maine with an apparatus described elsewhere.[13,14] These data are shown as open circles in Figure 2b.

Data of the temperature dependence of the luminescence lifetimes were fit according to eqs 1 and 2 (see below) with the CET NLLSQ 1.3 nonlinear least-squares program on an Apple II computer.[21] Proper weighting of the data was included.[22] All uncertainties reported in the parameters represent the standard deviations derived from such an analysis.

Computational Details

The calculations reported were of the extended Hückel type.[2a,b,5,6,14,19] The relativistic and nonrelativistic energy- and orbital-exponent parameters used are listed in Table I.[19] Charge iteration was used such that the change in H_{ii} was linearly related to the charge of the species. For the p- and d-orbital parameters the weighted average of the low and high angular momentum values of the relevant relativistic orbitals are given. Linear geometry was assumed for $Au(CN)_2^-$, and bond distances were taken to be the crystallographic values reported in the literature for $K[Au(CN)_2]$[11] and $Tl_2Pt(CN)_4$.[3]

Results

1. $Tl[Au(CN)_2]$ Spectra and Lifetimes. Figure 1a shows the luminescence spectrum of $Tl[Au(CN)_2]$ as a function of temperature from 5 to 360 K. At 5 K, two bands are present, one of low intensity at 17 390 cm^{-1} and one of high intensity at 19 285 cm^{-1}. The intensity of the 17 390-cm^{-1} band is seen to decrease with increase in temperature relative to the 19 285-cm^{-1} band. The 17 390-cm^{-1} band appears as a shoulder on the 19 285-cm^{-1} band at 40 K and is not present at 300 K and above. The 19 285-cm^{-1} band increases in intensity and shifts to 19 620 cm^{-1} from 5 to 40 K. From 40 to 360 K, the intensity of this band remains roughly constant but a further shift to higher energy occurs, reaching 20 670 cm^{-1} at 360 K.

The luminescence spectrum at 4.2 K and 6 T compared to that at 4.2 K and 0 T is shown in Figure 1b. A narrowing of the 19 285-cm^{-1} band and a shift of 240 ± 40 cm^{-1} to 19 525 cm^{-1} is seen relative to the spectrum at 0 T. In addition, the luminescence decay becomes nonexponential at 6 T as observed for $Cs[Au(CN)_2]$.[16] No change is seen in the intensity or energy of the weak 17 390-cm^{-1} band. The difference in integrated intensities of the spectra is less than 1%. The weak shoulder located at 18 800 cm^{-1} does not change in intensity or energy as the magnetic field is increased from 0 to 6 T. Furthermore, the intensity of this peak was found to vary with sample preparation and so is likely due to the presence of a small amount of impurity. In any event the lifetime of the band at 19 285 cm^{-1} is not affected by the intensity of this peak.

The temperature dependence of the lifetime of the 19 285-cm^{-1} band from 1.7 to 16 K is shown in Figure 2a. A dramatic increase in the lifetime is observed from the plateau at the lowest temperatures (τ = 168 μs) to 50 K (τ = 2.1 μs). Figure 2b shows the lifetime variation from 100 to 400 K. A substantial though smaller dropoff from the plateau at 100–250 K (τ = 210 ns) is seen at higher temperatures, leveling off to about 55 ns above 340 K. Monoexponential decays were observed at all temperatures.

2. Electronic Structure Calculations. (a) $Au(CN)_2^-$. Figure 3 shows the electronic structure of an isolated $Au(CN)_2^-$ ion obtained both by relativistic and nonrelativistic wave functions and assuming $D_{\infty h}$ symmetry. The $4\sigma_g$ orbital is the highest occupied molecular orbital (HOMO) in both cases. Compared to the nonrelativistic value, the $4\sigma_g$ orbital is slightly stabilized due to relativistic effects. However, the most noticeable difference between the relativistic and nonrelativistic results is the *composition* of the HOMO. The relativistic result shows a 71% contribution from Au (22% 6s, 49% $5d_{z^2}$) and only 29% from CN^- σ_p. The nonrelativistic result however gives only a 50% contribution from Au (mainly from 6s).

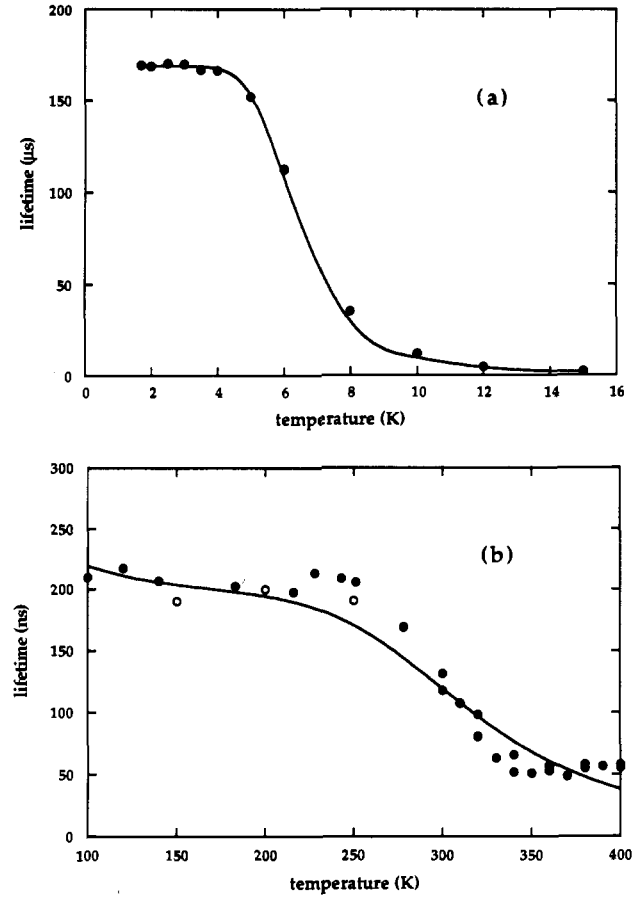

Figure 2. (a) Luminescent lifetimes of $Tl[Au(CN)_2]$ from 1.7 to 16 K following pulsed laser excitation at 25 100 cm^{-1}. The solid line drawn through the data (solid circles) was calculated from eq 1 with the parameters given in Table III. (b) Luminescence lifetimes of $Tl[Au(CN)_2]$ from 100 to 400 K following pulsed laser excitation at 25 100 cm^{-1}. The solid line drawn through the data obtained at Bowdoin College (solid circles) was calculated from these data according to eq 2 with the parameters given in Table III. Data obtained independently at University of Maine from a different sample of $Tl[Au(CN)_2]$ and with a different apparatus are shown as open circles.

The major consequences of relativistic effects are known to be a radial contraction and an energetic stabilization of s orbitals and a radial expansion and energetic destabilization of d orbitals.[2a,b,c] These effects result in better mixing between the 6s and $5d_{z^2}$ orbitals. Thus in $Au(CN)_2^-$ relativistic effects lead to 33% more $5d_{z^2}$ character in the HOMO. The overlap population of Au–C also increases to 0.37 from the nonrelativistic value of 0.24.

The effect of relativistic destabilization of the d orbitals as shown in Figure 3 causes a uniform increase in the energies of the $2\pi_g$, $1\delta_g$, and $3\sigma_g$ orbitals of $Au(CN)_2^-$. In contrast, the CN^- based $1\pi_u$ and $1\pi_g$ orbitals do not change significantly on going from the relativistic to the nonrelativistic situation.

The composition of the HOMO determined by considering relativistic effects on Au is consistent with the results of nonrelativistic discrete variational–Xα (DV–Xα) calculations,[23] the

(21) Christian, S. D.; Tucker, E. E. *Am. Lab.* **1982**, *14*(9), 31–34.
(22) Christian, S. D.; Tucker, E. E. *Am. Lab.* **1984**, *16*(2), 18–22.
(23) (a) Guenzburger, D.; Ellis, D. E. *Phys. Rev. B* **1980**, *22*, 4203–4214. (b) Sano, M.; Adachi, H.; Yamatera, H. *Bull. Chem. Soc. Jpn.* **1982**, *55*, 1022–1027. (c) Gutsev, G. *J. Struct. Chem.* (*Engl. Transl.*) **1988**, *29*, 670–674; *Zh. Strukt. Khim.* **1988**, *29*, 16–21.

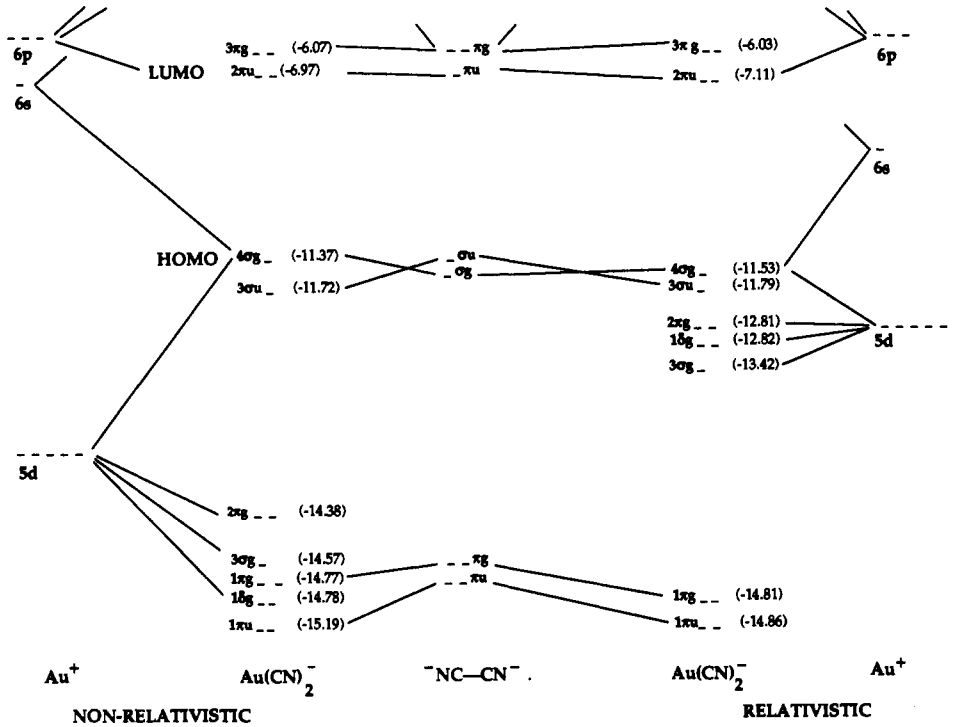

Figure 3. Electronic structure of $Au(CN)_2^-$ (shown as an orbital correlation diagram) as obtained from both relativistic and nonrelativistic extended Hückel calculations with $D_{\infty h}$ symmetry and the z axis taken to be the molecular axis. Relativistic effects cause the HOMO to show more than a 20% increase in the contribution from the Au $5d_{z^2}$ orbital.

corresponding DV-Xα values being 72% Au (40% 6s, 32% $5d_{z^2}$),[23a] 81% Au (34% 6s, 47% $5d_{z^2}$),[23b] and 85% Au.[23c] The results of relativistic and nonrelativistic Hartree–Fock calculations[2h] are also in agreement with these values. Substantial mixing of Au 6p orbitals with CN^- π^* orbitals is observed in the higher energy molecular orbitals. The lowest unoccupied molecular orbital (LUMO), $2\pi_u$, consists of 88% CN^- π^* and 12% Au 6p character (DV-Xα calculations give 73% Au 6p character[23a]). As found for the Pt–CN interaction in $Tl_2Pt(CN)_4$ studied previously[1] and for the DV-Xα calculations on $Au(CN)_2^-$,[23] negligible $6p_z$ participation in the bonding and very little Au 5d to CN^- π^* back-bonding is found. The negligible π back-bonding is in agreement with a recent nonrelativistic multiple-scattering-Xα (MS-Xα) study of $Au(CN)_2^-$,[24] but is in disagreement with a recent Hartree–Fock study.[2h] The Xα study as well as interpretations of Mössbauer studies on Au(I) compounds[8c,10d,25] concludes that there is substantial Au $6p_z$ involvement in the bonding, a result in contrast to that obtained here and in the DV-Xα calculations.[23] However, the limitations of MS-Xα calculations when applied to unsymmetrical molecules of this type have been noted,[1] as have the difficulties in interpreting Mössbauer results for two-coordinate gold(I) compounds.[2h]

Finally, the HOMO–LUMO energy separation calculated from the relativistic wavefunctions is 4.42 eV, in good agreement with the lowest energy transition of 5.18 eV observed experimentally and determined by DV-Xα calculations.[23a]

(b) Tl[Au(CN)$_2$]. Different orientations of Tl^+ with $Au(CN)_2^-$ were assessed, specifically Tl^+ bonding through a bridging CN^- and bonding directly to Au. The one-electron stabilization energy is found to be greater when Tl^+ bonds directly to Au. The orbitals involved in this case as calculated from the relativistic wave functions at a Tl–Au separation of 3.0 Å are presented in Figure 4 in C_{2v} point group notation. Here the y axis is defined as the NC–Au–CN axis and the z axis as the Tl–Au axis. A correlation table based on this axis convention (the "$z \rightarrow y$" case)[26] is helpful in following the orbital correlations shown in Figure 4. The 0.31 overlap population of Tl with Au at a 3.0-Å separation is small but positive. In accord with previous work,[2g] no interaction is observed between the Tl-based 5d orbitals and the π orbitals of the CN^- ligands. The most important interaction is that involving the empty $6p_z$ and filled 6s orbitals of Tl with empty π^* and filled σ orbitals of the CN^- ligands. The interaction of the Tl 6s orbital with the CN^- σ orbitals is reflected in the relatively low energy of the $6a_1$ Tl–Au(CN)$_2$ orbital. The HOMO ($9a_1$) has 60% Au (15% 6s, 45% $5d_{z^2}$) and 25% CN^- σ character.

Our calculations show that the composition of the HOMO remains the same at both large and small Tl–Au distances. The LUMO ($4b_1$) on the other hand has mostly CN^- π^* character (78%), the remaining portion containing Tl $6p_z$ and Au contributions. At shorter Tl–Au separations this LUMO incorporates more Tl $6p_z$ character (11% at 3.0 Å). The interaction between the Tl $6p_z$ and CN^- orbitals in Tl[Au(CN)$_2$] stabilizes the LUMO ($4b_1$) and destabilizes the HOMO ($9a_1$), thereby decreasing the HOMO–LUMO gap.

At a 3.0-Å Au–Tl separation the HOMO–LUMO gap is 0.4 eV smaller than that for the isolated $Au(CN)_2^-$ ion. These effects are clearly observable in Figure 4. The interaction of the Tl 6p orbitals with CN^- π^* orbitals lifts the degeneracy of the two ligand-based orbitals ($4b_1$ and $10a_1$). Both orbitals are stabilized in energy compared to the $Au(CN)_2^-$ ion.

The potential energy curves of Cs^+–$Au(CN)_2^-$ and Tl^+–$Au(CN)_2^-$ are shown in Figure 5a,b. For both Cs^+ and Tl^+ the 5d, 6s, and 6p valence orbitals were included in the calculation. The energy minimum at 3.0 Å for Tl^+–$Au(CN)_2^-$ and the lack of such a minimum for Cs^+–$Au(CN)_2^-$ support the possibility of covalent Tl–Au interactions in Tl[Au(CN)$_2$] but not in Cs[Au(CN)$_2$].

(c) $Pt(CN)_4^{2-}$ and $Tl_2Pt(CN)_4$. The results of relativistic extended Hückel electronic structure calculations on $Pt(CN)_4^{2-}$ and $Tl_2Pt(CN)_4$ are shown in Figure 6. For $Pt(CN)_4^{2-}$ the HOMO is a $5a_{1g}$ orbital consisting of 93% Pt $5d_{z^2}$ and 7% Pt 6s character. The LUMO ($3a_{2u}$) has 84% CN^- p_z and 16% Pt $6p_z$ character.

(24) Bowmaker, G. A.; Boyd, P. D. W.; Sorrenson, R. J. *J. Chem. Soc., Faraday Trans. 2* **1985**, *81*, 1627–1641.
(25) Jones, P. G.; Maddock, A. G.; Mays, M. J.; Muir, M. M.; Williams, A. F. *J. Chem. Soc., Dalton Trans.* **1977**, 1434–1443.
(26) Herzberg, G. *Molecular Spectra and Molecular Structure. III. Electronic Spectra and Electronic Structure of Polyatomic Molecules*; D. Van Nostrand: Princeton, NJ, 1966; p 576.

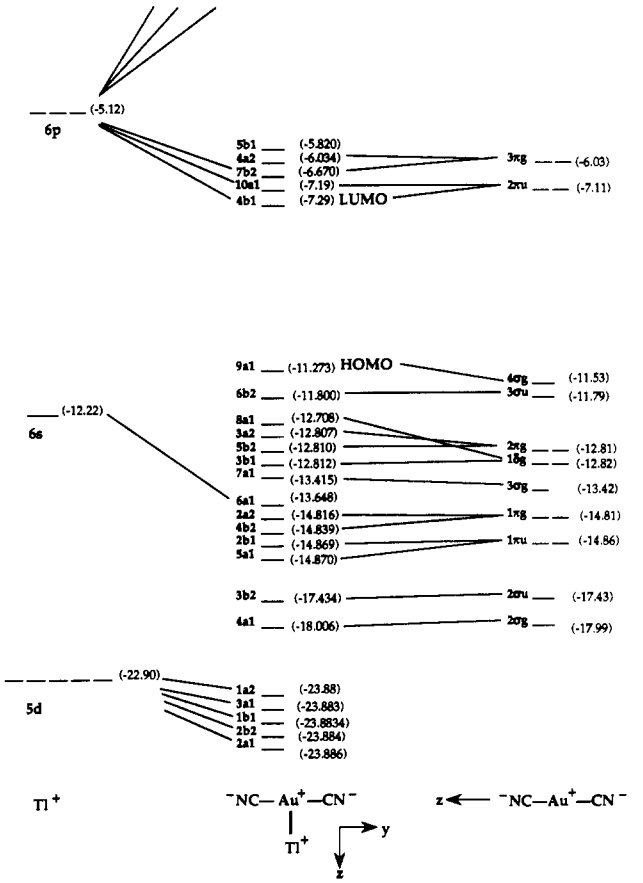

Figure 4. Electronic structure of Tl[Au(CN)$_2$] as obtained from a relativistic extended Hückel calculation at an Au–Tl separation of 3.0 Å. The symmetry was taken to be C_{2v} with the y axis defined as the NC–Au–CN axis and the z axis as the Tl–Au axis. Orbital correlations with the results of calculations for Tl^+ and $Au(CN)_2^-$ are shown and a correlation table based on this axis convention is available (the convention adopted here corresponds to the $D_{\infty h} \rightarrow C_{2v}$ "$z \rightarrow y$" case given in the table).[26] The energies (in eV) of Tl[Au(CN)$_2$] are given to three decimal places to facilitate comparisons between levels.

This, as well as the d-orbital ordering $5d_{x^2-y^2} \gg 5d_{z^2} > 5d_{xz,yz} > 5d_{xy}$, is in good agreement with recent relativistic density functional calculations.[1]

For $Tl_2Pt(CN)_4$ the HOMO ($7a_{1g}$) consists of 82% Pt $5d_{z^2}$ and 18% CN^- σ contributions while the LUMO ($3a_{2u}$) has 66% CN^- π^* and 33% Tl p_z orbital character. Relativistic density functional calculations[1] on $Tl_2Pt(CN)_4$ also give an a_{2u} LUMO but with 14% CN^- π^*, 74% Tl $6p_z$, and 11% Pt $6p_z$ character (all values given from the density functional calculation[1] and the spin–orbit-averaged quasi-relativistic results). This mixing of the Tl valence orbitals with the $Pt(CN)_4^{2-}$ valence orbitals in the density functional calculations is also evident in the ordering of the Pt 5d-based orbitals in $Tl_2Pt(CN)_4$ relative to $Pt(CN)_4^{2-}$ (compare with Figures 1 and 3 of ref 1). In fact the HOMO in the density functional calculations is the $3b_{2g}$ orbital, which is 0.64 eV above the highest occupied a_{1g} orbital, $7a_{1g}$, which has 77% CN^- σ, 15% Pt $5d_{z^2}$, 2% Pt 6s, and 3% Tl $6p_z$ character.[1] The $6a_{1g}$ lies 1.55 eV below the HOMO and has 39% Pt $5d_{z^2}$, 14% Pt 6s, 23% Tl $6p_z$, and 23% CN^- σ character.[1]

Such substantial mixing with the Tl orbitals is not found in the relativistic extended Hückel calculations. Assuming the density-functional calculations represent a more accurate picture of the bonding between Tl^+ and $Pt(CN)_4^{2-}$ than the extended Hückel calculations, then the extent of mixing between Tl^+ and $Au(CN)_2^-$ or $Pt(CN)_4^{2-}$ reported here can be taken as a lower limit to such interactions.

(d) [Au(CN)$_2^-$]$_2$ and [Au(CN)$_2^-$]$_3$. Figure 7 shows the electronic structure obtained from the relativistic extended Hückel calculation for the $[Au(CN)_2^-]_2$ dimer. The z axis is the Au–CN axis for the $Au(CN)_2^-$ monomers and the Au–Au axis for the $[Au(CN)_2^-]_2$ dimer. This corresponds to the "$z \rightarrow x$" case listed in $D_{\infty h} \rightarrow D_{2h}$ correlation tables.[26]

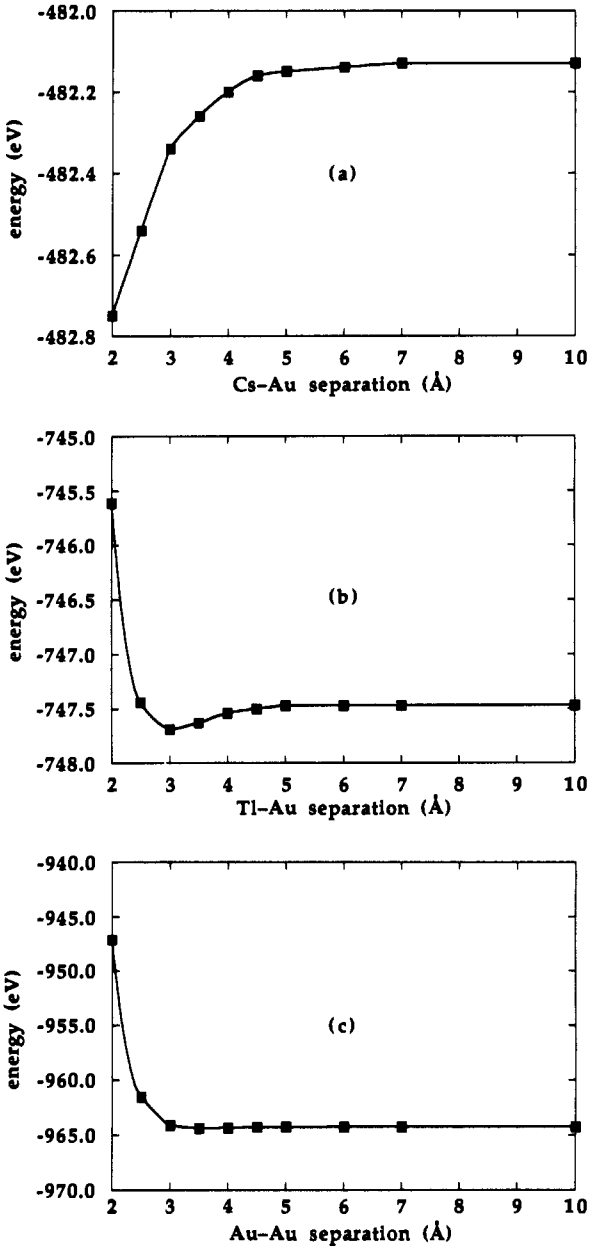

Figure 5. Potential energy curves of (a) Cs^+–$Au(CN)_2^-$, (b) Tl^+–$Au(CN)_2^-$, and (c) $Au(CN)_2^-$–$Au(CN)_2^-$ as obtained from relativistic extended Hückel calculations.

The basic features of the electronic structure remain the same as for the monomer. At an Au–Au separation of 3.5 Å the HOMO of the dimer ($6a_g$) consists of 70% Au (20% 6s and 50% $5d_{z^2}$) and 30% CN^- σ_p character. Compared to that for the monomer the d_{z^2} contribution to the HOMO is slightly increased and the 6s contribution is decreased. The LUMO ($7b_{1u}$) consists of 10% Au $6p_z$ and 90% CN^- p_z character. Like those in the monomer, important interactions in the dimer are found between the filled $5d_{z^2}$ and empty 6s Au orbitals and the σ and π^* CN^- orbitals. The Au–Au bonding mainly involves 6s and $5d_{z^2}$ interactions, with little participation of $6p_z$ orbitals. The lack of $6p_z$ involvement is in accord with SCF–Xα–SW calculations reported recently for a phosphine-bridged Au dimer.[10g]

At short Au–Au distances, the contribution to the HOMO from Au $5d_{z^2}$ increases. The HOMO–LUMO separation also decreases proportionately with decreasing Au–Au separation (3.79 vs 3.36 eV at 3.5 and 3.019 Å, respectively). At an Au–Au separation of 3.5 Å, the overlap population is 0.022. Although this value is positive, it is only about one-tenth of the value obtained for the

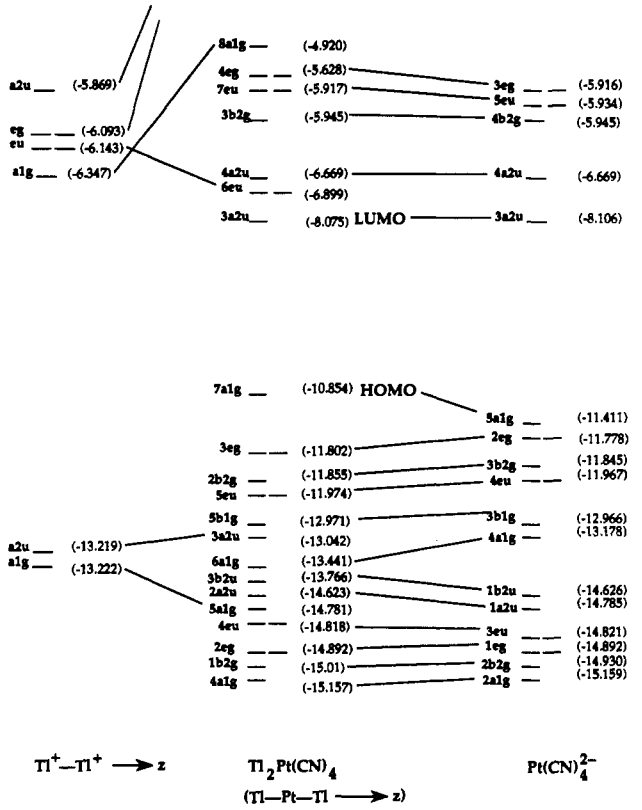

Figure 6. Electronic structures of $Tl_2Pt(CN)_4$ and $Pt(CN)_4^{2-}$ (D_{4h} symmetry; z axis defined as the Tl–Pt–Tl axis) as obtained from relativistic extended Hückel calculations and shown as an orbital correlation diagram. Notice that the energy ordering of the Pt 5d-based molecular orbitals is the same in both cases ($a_{1g} > e_g > b_{2g}$). Energies (in eV) are given to three decimal places to facilitate comparisons between levels.

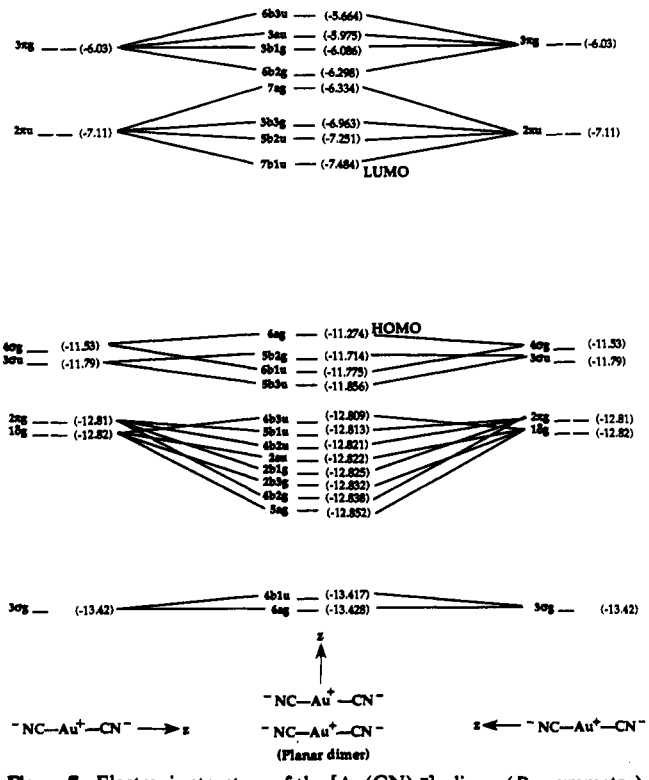

Figure 7. Electronic structure of the $[Au(CN)_2^-]_2$ dimer (D_{2h} symmetry) as obtained from a relativistic extended Hückel calculation and shown as an orbital correlation diagram. The z axis is the Au–CN axis for the monomers and the Au–Au axis for the $[Au(CN)_2^-]_2$ dimer. This corresponds to the "$z \rightarrow x$" case listed in $D_{\infty h} \rightarrow D_{2h}$ correlation tables.[26] Energies (in eV) are given to three decimal places to facilitate comparisons between levels.

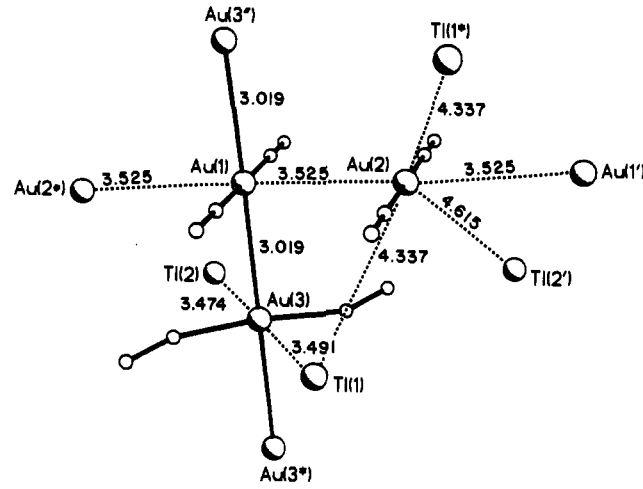

Figure 8. Atomic positions for Au and Tl atoms in crystalline Tl[Au(CN)$_2$] as determined by X-ray crystallography at 125 K.[27] It is proposed that the observed luminescence results from both Au–Au and Tl–Au interactions along the axis defined by the Au(1) and Au(3) sites. Notice the substantially longer Au–Au and Tl–Au separations in the Au(2) sites. Values of all distances shown are in ångstroms.

Au–Tl interaction in Tl[Au(CN)$_2$]. Only small interactions are observed among the other orbitals.

Calculations were also carried out for the trimer $[Au(CN)_2^-]_3$. Compared with the case of the dimer, in the trimer the Au 6s orbital contribution to the Au–Au interactions decreases while that from the $5d_{z^2}$ orbital increases. The overlap population also decreases to 0.011 at an Au–Au separation of 3.5 Å. The HOMO–LUMO gap decreases by 10% on going from dimer to trimer. In both the dimer and trimer, shorter Au–Au separations decrease the HOMO–LUMO gap and increase the d_{z^2} participation in the HOMO. In the case of the trimer, 50% of the Au contribution to the HOMO arises from the central Au atom and 25% from each of the two terminal Au atoms 3.019 Å away.

Figure 5c shows the potential energy curve obtained for $[Au(CN)_2^-]_2$ as a function of distance between the Au atoms. Note the shallow minimum at 3.5 Å. This relatively long Au–Au distance is further evidence of a weak Au–Au covalent interaction.

Discussion

1. Absorption and Luminescence Spectra of Tl[Au(CN)$_2$]. The isostructural compounds Tl[Au(CN)$_2$] and Cs[Au(CN)$_2$][12] show substantial differences in their optical properties. Most obvious is the difference in the appearance of the crystals. Whereas Cs[Au(CN)$_2$] is colorless (except for a faint violet tinge due to its luminescence), Tl[Au(CN)$_2$] is a bright canary yellow. Since the low-energy absorption and luminescence of crystalline Cs[Au(CN)$_2$] have been postulated to be due to Au–Au interactions,[15,16] it is surprising that such a marked difference in the color of crystalline Tl[Au(CN)$_2$] is found since the shortest Au–Au separation in Tl[Au(CN)$_2$] is only 0.07 Å less than that in the isostructural Cs[Au(CN)$_2$].[12]

This observation has led to the suggestion that interactions between thallium and gold atoms lower both the absorption and luminescence energies in Tl[Au(CN)$_2$].[18] The crystal structure of Tl[Au(CN)$_2$] at 298 K as determined by neutron diffraction[12] shows Tl–Au separations of 3.446 and 3.463 Å at one of the three crystallographically distinct Au sites in the crystal. Figure 8 (drawn from X-ray data at 125 K[27]) shows these sites and the various Au–Au and Tl–Au separations for each. It is likely that the luminescence at 21 830 cm^{-1} in Cs[Au(CN)$_2$] and at 19 285 cm^{-1} in Tl[Au(CN)$_2$] results from transitions at trapped Au(3) sites localized along the Au(1)–Au(3) chain since those sites exhibit the closest average Au–Au separations. The lowering in energy of the luminescence of Tl[Au(CN)$_2$] relative to that for Cs[Au(CN)$_2$] is likely due to interactions between Tl and Au at the Au(3) sites in the Au(1)–Au(3) chain since the Au–Au

(27) Nagle, J. K.; Balch, A. L.; Olmstead, M. M. Unpublished results.

Table II. Results of Relativistic Extended Hückel Calculations of the HOMO–LUMO Energy Separation and Total Energy for an $Au(CN)_2^-$ Ion Interacting with Adjacent $Au(CN)_2^-$ Ions (Au) and Tl^+ Ions (Tl).

site	interaction	HOMO–LUMO gap, eV	tot. energy, eV
1	2Au(2,2*), 3.525 Å; 2Au(3,3''), 3.019 Å	2.65	−2416.45[b]
2	2Au(1,1'), 3.525 Å; 2Tl(1,1*), 4.337 Å	3.45	−1980.77
3	2Au(1,3*), 3.019 Å; 2Tl(1,2), 3.490 Å	2.66	−1980.67

[a] The labels given in parentheses correspond to the crystallographic notion used in Figure 8. [b] The CN^- ions surrounding the Au(3,3*) site were taken into consideration in the calculation for this site, which leads to a much lower total energy for this site in comparison to the other two.

separations are about the same in these isostructural compounds.[12] Perhaps the most convincing evidence that Tl interactions with 5d metal atoms influence the luminescence of solid metal cyanides comes from studies of $Tl_2Pt(CN)_4$, which show it to have a luminescence band at 4.2 K centered at 21 950 cm^{-1}.[3,20]

The extended Hückel calculations on isolated $Tl[Au(CN)_2]$ and $Cs[Au(CN)_2]$ molecules incorporating relativistic effects for Au and Tl atoms substantiate this postulate. Table II lists the one-electron total energy and HOMO–LUMO separation obtained from relativistic extended Hückel calculations for models of the three crystallographically distinguishable sites in $Tl[Au(CN)_2]$. Notice the small calculated HOMO–LUMO gap at site Au(3) for $Tl[Au(CN)_2]$ despite the fact that, as pointed out above, these calculations may provide only a lower limit to the Tl–Au interactions. The lowering in energy of both the absorption and luminescence of $Tl[Au(CN)_2]$ compared to $Cs[Au(CN)_2]$ can then be ascribed to Tl–Au interactions at the Au(3) sites along the Au(1)–Au(3) chain. In contrast, calculations show that the presence of Cs at site Au(3) *increases* the Au–Au interaction. The Au–Au overlap population increases from 0.001 to 0.028 when Tl is replaced by Cs. Another effect of replacing Tl by Cs is that the HOMO–LUMO gaps at sites Au(3) and Au(2) in $Cs[Au(CN)_2]$ become essentially the same (3.43 eV) while for $Tl[Au(CN)_2]$ gaps of 2.66 and 3.45 eV, respectively, are calculated.

The covalent bonding between Tl and Au is clearly observed since Tl, by withdrawing electron density, decreases the Au–Au interaction while Cs shows an opposite effect. Furthermore, Figure 5 shows clearly the enhanced interaction between Tl and Au as compared to that for Au and Cs (which exhibits only ionic interactions), and the calculation on $[Au(CN)_2^-]_2$ (Figure 5c) shows that at 3.00 Å the Au–Au interaction is much weaker than the Tl–Au interaction in $Tl[Au(CN)_2]$ (Figure 5b). Finally, Tl–Au interactions have been found in the molecular compound $TlAu[(C_6H_5)_2P(CH_2)S]_2$,[28] and the influence of relativistic effects in promoting this interaction have been noted.[28]

Another striking difference between $Tl[Au(CN)_2]$ and $Cs[Au(CN)_2]$ occurs at low temperatures. In addition to the long-lived 21 830-cm^{-1} band of $Cs[Au(CN)_2]$ at 5 K, a second strong but short-lived ($\tau < 5$ ns) band at 24 040 cm^{-1} is observed (see Figure 1 of ref 16). This has been attributed to fluorescence from a singlet state,[16] perhaps of delocalized nature with respect to the Au(1)–Au(3) chain interactions and analogous to the luminescence spectra of columnar $Pt(CN)_4^{2-}$ compounds.[29] No such band is observed for $Tl[Au(CN)_2]$. If the initially populated singlet states in $Cs[Au(CN)_2]$ and $TlAu(CN)_2$ decay via both luminescence (at 24 040 and 19 285 cm^{-1}, respectively) and nonradiative decay to the spin–orbit split triplet state, then a more rapid singlet–triplet interconversion in $Tl[Au(CN)_2]$ relative to $Cs[Au(CN)_2]$ could explain the lack of fluorescence in $Tl[Au(CN)_2]$. The presence of Tl atoms presumably facilitates a more rapid singlet–triplet interconversion. Additional evidence that this is so comes from the luminescence lifetime results as discussed below.

The 335 ± 30 cm^{-1} shift of the 19 285 cm^{-1} band at 4.2 K to 19 620 cm^{-1} at 40 K is analogous to the 380-cm^{-1} shift observed

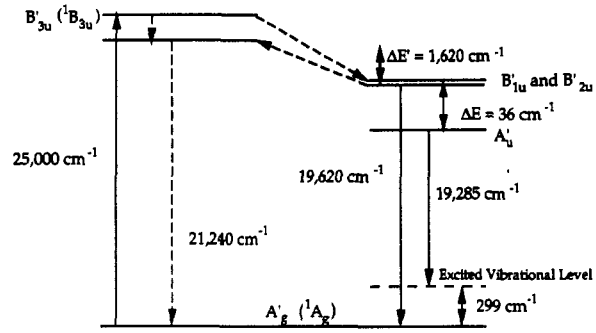

Figure 9. Simplified energy level diagram based on D_{2h} symmetry representing the various levels and transitions involved in microcrystalline $Tl[Au(CN)_2]$ following pulsed laser excitation at 25 100 cm^{-1}. The levels are not drawn to scale. The reverse intersystem crossing from the nearly degenerate B'_{1u} and B'_{2u} levels to the lower of the two nonluminescent B'_{3u} ($^1B_{3u}$) vibrational levels is postulated to be responsible for the decrease in lifetime seen in Figure 2b. Mixing of the A'_u state with the B'_{1u} and B'_{2u} states accounts for the observed magnetic field effects.

over a similar temperature range for $Cs[Au(CN)_2]$,[15,16] and the model used to explain these results (Figure 9) is essentially the same as that used for $Cs[Au(CN)_2]$.[15,16] Thus, as the temperature increases over this range, thermal population of the degenerate B'_{1u} and B'_{2u} states lying 36 cm^{-1} higher in wavenumber (this value is derived from an analysis of the luminescence lifetime results as described below) occurs. That the observed shift is about 10 times as large as this value is a result of the fact that the decay from the A'_u state to the A'_g ground state is symmetry forbidden and so the observed decay is to an excited vibrational level.[17] In contrast, the B'_{1u} and B'_{2u} to A'_g transitions are symmetry allowed and occur directly to the vibrational ground level. Therefore the difference (335 ± 30 cm^{-1}) − 36.0 cm^{-1} = 299 ± 30 cm^{-1} should correspond to the energy of an excited vibrational level of the A'_g ground electronic state. Infrared and Raman bands are observed in the 290–319-cm^{-1} region of the spectrum of $Tl[Au(CN)_2]$,[17] the next highest and lowest energy vibrations occurring at 389 and 178 cm^{-1}, respectively. The energy levels and various transitions involved in the excited state processes are summarized in Figure 9.

It might be expected that the two bands should be observable at temperatures between about 4 and 10 K where the steep drop in lifetime occurs (Figure 2a). However, at 5 K only a minor component of the 19 620-cm^{-1} band is expected to be present since the lifetime has dropped only about 10% from the 167-μs plateau at lower temperatures. Furthermore, the 19 620-cm^{-1} band is shifted only 335 cm^{-1} from the 19 285-cm^{-1} band, and both bands are broad (widths ≈ 800 cm^{-1}). Therefore, two distinct peaks are not expected to be noticeable at this temperature. At 40 K the lifetime data predict that, as observed, only the 19 620-cm^{-1} band should be present.

The weak 17 390-cm^{-1} luminescence of $Tl[Au(CN)_2]$ at low temperatures is probably due to luminescent traps caused by imperfections in the microcrystalline samples used. In support of this suggestion, the temperature dependence of this band is very different from the 19 285-cm^{-1} band (Figure 1a), and both the intensity and energy are unchanged in the presence of a 6-T magnetic field, in contrast to the behavior of the 19 285-cm^{-1} band (Figure 1b). The intensity of the 17 390-cm^{-1} band was too low to make reliable lifetime measurements.

The effects of a magnetic field on the luminescence of $Tl[Au(CN)_2]$ are completely in accord with the model used for $Cs[Au(CN)_2]$.[16] The 240 ± 40 cm^{-1} blue shift of the luminescence as the magnetic field is increased from 0 to 6 T at 4.2 K is explained by the field-induced mixing of the B'_{1u} and B'_{2u} states with the A'_u state.[30] In the absence of such mixing, luminescence at 4.2 K results from decay from the A'_u level to an excited vibrational level about 299 cm^{-1} above the ground state. No detailed analysis of the magnetic field effects as reported for

(28) Wang, S.; Fackler, J. P., Jr.; King, C.; Wang, J. C. *J. Am. Chem. Soc.* **1988**, *110*, 3308–3310.
(29) Gliemann, G.; Yersin, H. *Struct. Bonding* **1985**, *62*, 87–153.
(30) Gliemann, G. *Comments Inorg. Chem.* **1986**, *5*, 263–284.

Table III. Numerical Values of the Parameters Characterizing the Luminescence Decays of Tl[Au(CN)$_2$], Cs[Au(CN)$_2$], Tl$_2$Pt(CN)$_4$, and K$_2$[Pt(CN)$_4$] from 1.4 to 300 K[a]

param	Tl[Au(CN)$_2$]	Cs[Au(CN)$_2$]	Tl$_2$Pt(CN)$_4$[b]	K$_2$[Pt(CN)$_4$][c]
temp range, K	1.7–400[d]	1.6–300	1.7–38.7	1.7–41.5
ΔE, cm^{-1}	36.0 ± 0.4	45.22 ± 0.03	44.8 ± 2.4	56.5 ± 5.1
k_1, s^{-1}	(5.94 ± 0.03) × 10^3	(1.636 ± 0.002) × 10^3	(1.29 ± 0.02) × 10^4	(2.35 ± 0.12) × 10^2
k_2, s^{-1}	(8.4 ± 0.3) × 10^6	(2.07 ± 0.03) × 10^6	(7.0 ± 0.7) × 10^5	(2.4 ± 0.5) × 10^6
$\Delta E'$, cm^{-1}	1620 ± 210			
k_3, s^{-1}	(1.9 ± 1.6) × 10^{10}			

[a] The parameters are defined by eq 1 (Cs[Au(CN)$_2$] and Tl$_2$Pt(CN)$_4$) and eq 2 (Tl[Au(CN)$_2$]) in the text and were obtained by weighted, non-linear least squares analyses of the luminescence decay rates for the three compounds. [b] Data from ref 20. [c] Data from ref 32. [d] The values of ΔE and k_1 in eq 2 for Tl[Au(CN)$_2$] were determined from data in the range 1.7–240 K with eq 1. $\Delta E'$, k_2, and k_3 were determined from data over the entire temperature range listed with eq 2 and with fixed values of ΔE and k_1.

Cs[Au(CN)$_2$][16] was attempted.

2. Luminescence Lifetimes of Tl[Au(CN)$_2$]. The lifetimes of the luminescence in the 19 000–21 000-cm^{-1} range from 1.7 to 250 K (Figure 2) were fit according to eq 1. This equation is derived

$$\tau = (1 + 2e^{-\Delta E/kT})/(k_1 + 2k_2e^{-\Delta E/kT}) \quad (1)$$

on the assumption that the luminescence occurs from two levels in Boltzmann equilibrium with each other and separated by an energy ΔE. The rate constants k_1 and k_2 correspond to decay from the lower and upper levels, respectively. The scheme shown in Figure 9 identifies the lower luminescing level with the excited A'_u electronic state and the upper one with the degenerate B'_{1u} and B'_{2u} excited electronic states. In this model the rate constant k_1 corresponds to the decay from A'_u to an excited vibrational state of the ground electronic state A'_g while k_2 corresponds to decay from B'_{1u} and B'_{2u} to the ground vibrational state of the electronic state A'_g. The values of the parameters k_1, k_2, and ΔE derived by fitting the lifetime data to eq 1 are given in Table III. Analogous values derived for Cs[Au(CN)$_2$] are also given for purposes of comparison.

The values of the rate constants k_1 and k_2 increase by factors of 3.6 and 4.1, respectively for Tl[Au(CN)$_2$] compared to Cs[Au(CN)$_2$] while ΔE decreases from 45.2 to 36.0 cm^{-1}. Since the k_1 and k_2 decay pathways presumably involve—at least formally—a triplet to singlet conversion, the increase in these values for Tl[Au(CN)$_2$] compared to Cs[Au(CN)$_2$] appears to be consistent with the lack of fluorescence for Tl[Au(CN)$_2$] since intersystem crossing also involves singlet to triplet conversions and intersystem crossing competes with fluorescence as a singlet-state pathway for deactivation. In fact, the observed increases in k_1 and k_2 should be viewed as lower limits to the effect of the Tl atoms on these rate constants. This is because, at least for compounds of Pt(CN)$_4^{2-}$, shorter metal–metal separations favor smaller decay rate constants,[29] and the Au(1)–Au(3) separation in Tl[Au(CN)$_2$] is 0.07 Å shorter than in Cs[Au(CN)$_2$].[12] Therefore k_1 and k_2 are expected to be smaller for Tl[Au(CN)$_2$] relative to Cs[Au(CN)$_2$] on the basis of the relative Au–Au separations in these compounds.

The smaller spin–orbit splitting ΔE between the A'_u and the nearly degenerate B'_{1u} and B'_{2u} states for Tl[Au(CN)$_2$] is possibly a result of the shorter Au–Au separations found in Tl[Au(CN)$_2$] relative to Cs[Au(CN)]$_2$. This type of effect has been discussed previously for K$_4$[Pt$_2$(P$_2$O$_5$H$_2$)$_4$][31] and is observed in compounds of Pt(CN)$_4^{2-}$ also.[29] The behavior of the luminescence of Tl$_2$Pt(CN)$_4$ at low temperatures[20] is similar to that observed for Tl[Au(CN)$_2$] and the corresponding parameters are also reported in Table III for purposes of comparison. The 20.7% decrease in ΔE for Tl$_2$Pt(CN)$_4$ relative to the value for K$_2$[Pt(CN)$_4$] (56.5 ± 5.1 cm^{-1})[32] is nearly the same as the 20.4% decrease for Tl[Au(CN)$_2$] relative to Cs[Au(CN)$_2$].

The additional decrease in lifetime for Tl[Au(CN)$_2$] at temperatures above 240 K, which is shown in Figure 2b, is not observed for Cs[Au(CN)$_2$]. Such a decrease suggests the presence of a higher energy, short-lived state that is thermally populated from the lower energy 20 400–20 800-cm^{-1} luminescent state. In fact the data over the entire temperature range from 1.7 to 400 K can be satisfactorily fit to the three-level equation[33]

$$\tau = (1 + 2e^{-\Delta E/kT} + e^{-\Delta E'/kT})/(k_1 + 2k_2e^{-\Delta E/kT} + k_3e^{-\Delta E'/kT}) \quad (2)$$

where the parameters ΔE, k_1 and k_2 are the same as in the two-level scheme used to account for the data in the 1.7–250 K range. $\Delta E'$ represents the difference in energy between the long-lived degenerate B'_{1u} and B'_{2u} states and the higher energy, short-lived state, which decays to the ground state with a rate constant represented by k_3.

A weighted, nonlinear least-squares analysis of the data was carried out by using fixed values for ΔE and k_1 determined from the two-level fit of the 1.7–240 K data (the same as the values listed in Table III). Such an analysis yields $\Delta E'$ = 1620 ± 210 cm^{-1}, k_2 = (8.4 ± 0.3) × 10^6 s^{-1}, and k_3 = (1.9 ± 1.6) × 10^{10} s^{-1}. The line calculated from these values is shown along with the experimental data in Figure 2b.

There are several reasons why the fit of the data in this higher temperature range is not as good as that at lower temperatures (Figure 2a). First, the observed lifetime varies by only a factor of 4 over the temperature range 40–400 K, and the experimental uncertainties in the data are larger than those for the much longer values at lower temperatures. Second, it is likely that $\Delta E'$ is not really constant but varies in proportion to the 1000-cm^{-1} change in the energy of the luminescence from 40 to 360 K. Third, the likely variation of $\Delta E'$ should lead to a variation in the rate constants for the nonradiative decay processes as a result of the energy-gap law.

Some additional lifetime data in this temperature region were obtained independently at the University of Maine and are shown as open circles in Figure 2b. These data, along with the scatter seen in the other data, indicate that the experimental uncertainty in the data in this region is about the same magnitude as the deviations between the experimental data and the calculated values represented by the solid line in the figure. These deviations are clearly not random; whether the systematic deviations observed are experimental in nature or represent a departure from the postulated model can only be answered by more accurate lifetime measurements in this temperature region.

It is likely that the higher lying state could be the nonluminescent $^1B_{3u}$ (B'_{3u} in double-group notation) delocalized fluorescent state (see Figure 9). For Cs[Au(CN)$_2$] the difference in energy between the low-energy triplet luminescence (trapped sites) and the high-energy singlet luminescence (chain delocalized) is 1890 cm^{-1} at 80 K, and a value of 2270 cm^{-1} is observed for K[Au(CN)$_2$] from time-resolved photoluminescence spectra at 5 K.[34] These values can be used as rough estimates for the energy difference between the singlet and triplet states in Tl[Au(CN)$_2$] at high temperatures. The 1620-cm^{-1} value is thus not unreasonable for this energy difference in Tl[Au(CN)$_2$]. Similar values are found for compounds of Pt(CN)$_4^{2-}$ and are known to vary with

(31) Reisch, G. A.; Turner, W. A.; Corson, M. R.; Nagle, J. K. *Chem. Phys. Lett.* **1985**, *117*, 561–565.
(32) Nagle, J. K.; Corson, M. R.; Dolan, P. J., Jr.; LaCasce, J. Unpublished results.
(33) Hager, G. D.; Crosby, G. A. *J. Am. Chem. Soc.* **1975**, *97*, 7031–7037.
(34) Nagle, J. K.; Corson, M. R.; Kopp, M. W. Unpublished results.

Pt-Pt separation.[29] The absence of such an effect for isostructural $Cs[Au(CN)_2]$ strongly suggests that the 1620-cm^{-1} energy gap in $Tl[Au(CN)_2]$ does not correspond to population of a higher vibronic state.

Thermal population (reverse intersystem crossing—the same type of process leading to delayed fluorescence) of the $^1B_{3u}$ (B'_{3u}) state delocalized along the Au(1)-Au(3) chain is a reasonable interpretation of this decrease in lifetime from 100 to 400 K (Figure 2b). The 30-330-ps estimate for the lifetime of this state ($=1/k_3$) is consistent with the value $\tau \leq 300$ ps determined for compounds of $Pt(CN)_4^{2-}$ in which delayed fluorescence is often observed.[29] It is unlikely that the observed decrease in lifetime in this temperature range is a result of a structural change as the structures at 298[12] and 125 K[27] are very similar, and no evidence for a phase transition between these temperatures was found.

Conclusions

The spectroscopic and theoretical results described above for $Tl[Au(CN)_2]$ show that substantial Au-Tl interactions are present in this compound. These interactions influence the energies, intensities, and rates of deactivation of the various states involved in the absorption and luminescence processes. The relatively strong Tl-Au interactions appear to be responsible for the lowering of the absorption and luminescence energies in $Tl[Au(CN)_2]$ relative to $Cs[Au(CN)_2]$.

The isostructural compound $Cs[Au(CN)_2]$ is useful for comparative purposes since no covalent Cs-Au interactions are evident either in its spectroscopic properties or in electronic structure calculations of it. Relativistic effects are demonstrated to play an important role in the Tl-Au interactions by influencing the relative 6s and 6p orbital energies of both Tl and Au.

Acknowledgment. Funds from a DuPont College Science Grant to the Bowdoin Department of Chemistry were used to purchase the laser. We thank Warren Turner and Paul Dolan, Jr., for help with the lifetime measurements, Dale Syphers for help with the magnetic field measurements, and David Roberts for help with data file conversions.

Contribution from the Isotope and Nuclear Chemistry Division and Nuclear Materials Technology Division, Los Alamos National Laboratory, Los Alamos, New Mexico 87545

Extension of Molecular Mechanics to High-Coordinate Metal Complexes. Calculation of the Structures of Aqua and Nitrato Complexes of Lanthanide(III) Metal Ions

Benjamin P. Hay*

Received October 2, 1990

Molecular mechanics methods have been used to calculate the diverse geometries found in 58 known structures of 8- to 12-coordinate aqua- and nitratolanthanide(III) complexes. A simple model based on the replacement of L-M-L bending interactions with nonbonded interactions between the ligand donor atoms and the use of harmonic M-L stretching potentials is shown to yield very reasonable geometric results. A method of structure specification for coordination compounds is presented that allows these calculations to be carried out by using the MM2 program without requiring any software modification.

Molecular mechanics calculations are becoming increasingly important in the area of coordination chemistry.[1] A continuing challenge has been the development of potential functions for metal-ligand interactions that are capable of generating the varied geometries found in d- and f-block metal complexes. Several methods have been devised to obtain the desired structures, but these methods have only been tested on a limited number of low-coordination-number geometries. The aim of the present study was to determine if existing molecular mechanics methodology could be used to calculate the diverse geometries encountered in high-coordinate metal complexes.

The most common method used to specify geometry about the metal ion has been to apply the potential functions of standard organic force fields.[2] Strain-free L-M-L bond angles are defined such that deformations from these strain free values result in an increase in energy. Such conventional force fields have been successfully employed to generate the geometries about the metal in tetrahedral, square-pyramidal, trigonal-bipyramidal, and octahedral Zn(II)[3] and Co(II)[3c] complexes; square-planar and square-pyramidal Cu(II) complexes;[4] square-planar and trigonal-bipyramidal Ni(II) complexes;[5] octahedral complexes of Co(III),[6] Ni(II),[7] and Rh(II);[8] and a hexagonal-bipyramidal complex of Sn(II).[9]

While the conventional approach of defining strain-free L-M-L bond angles is, in theory, applicable to any geometry, it becomes more difficult to implement as the number of ligands increases. The problem is that the number of strain free angles to be defined becomes large, e.g. 21 in a 7-coordinate complexes up to 66 in a 12-coordinate complex. A different set of angles would be required for each of the many possible geometries. In addition, the extent of programming required to ensure the correct assignment of a given strain-free L-M-L angle from a choice of

Table I. Metal-Independent Parameters

bond	k_r, mdyn Å^{-1}	r_0, Å	bond	k_r, mdyn Å^{-1}	r_0, Å
H—O	4.60	0.941	N=O	11.33	1.219
N—O	9.63	1.255			

angle	k_θ, mdyn Å rad^{-2}	θ_0, deg	angle	k_θ, mdyn Å rad^{-2}	θ_0, deg
H—O—H	0.300	109.0	O—N=O	0.700	121.6
H—O—M	0.300	125.5	O—N—M	0.000	0.0
O—N—O	0.700	116.8	out-of-plane about sp^2 nitrogen	0.050	0.0

torsion angle	V_2, kJ/mol	torsion angle	V_2, kJ/mol
O—N—O—M	18.83	O=N—O—M	18.83

nonbonded	ϵ, kJ/mol	d, Å	nonbonded	ϵ, kJ/mol	d, Å
H	0.197	1.50	O(N=O)	0.276	1.74
O(aqua)	0.209	1.74	N	0.230	1.82
O(N—O)	0.209	1.74	M	0.000	2.50

* Correspondence should be addressed to Battelle Pacific Northwest Laboratories, MS K6-81, PO Box 999, Richland, WA 99352.

(1) (a) Brubaker, G. R.; Johnson, D. W. *Coord. Chem. Rev.* **1984**, *53*, 1. (b) Hancock, R. D. *Prog. Inorg. Chem.* **1989**, *36*, 187. (c) Hancock, R. D.; Martell, A. E. *Chem. Rev.* **1989**, *89*, 1875.
(2) (a) Allinger, N. L. *Adv. Phys. Org. Chem.* **1976**, *13*, 1. (b) Burkert, U.; Allinger, N. L. *Molecular Mechanics*; ACS Monograph 177; American Chemical Society: Washington, DC, 1982. (c) Niketic, S. R.; Rasmussen, K. *The Consistent Force Field*; Springer: New York, 1977. (d) Rasmussen, K. *Potential Functions in Conformational Analysis*; Springer: New York, 1985.
(3) (a) Vedani, A.; Dobler, M.; Dunitz, J. D. *J. Comput. Chem.* **1986**, *7*, 701. (b) Vedani, A.; Huhta, D. W.; Jacober, S. P. *J. Am. Chem. Soc.* **1989**, *111*, 4075. (c) Vedani, A.; Huhta, D. W. *J. Am. Chem. Soc.* **1990**, *112*, 4759.

0020-1669/91/1330-2876$02.50/0